TEHRAN UNIVERSITY OF MEDICAL SCIENCES

IJOH INTERNATIONAL JOURNAL OF OCCUPATIONAL HYGIENE

eISSN: 2008-5435

IRANIAN OCCUPATIONAL HEALTH ASSOCIATION IOHA

ORIGINAL ARTICLE

Computational Fluid Dynamics Simulation of Airflow and Air Pattern in the Living Room for Reducing Coronavirus Exposure

KHOSRO ASHRAFI[1], HAMZEH MOHAMMADI[2], MAJID BAYATIAN[3*], ZAHRA AMIRI[3], ELAHE JAFARI[3]

[1]*School of Environment, College of Engineering, University of Tehran, Tehran, Iran*

[2]*Faculty of Health and Medical Engineering, Tehran Medical Sciences, Islamic Azad University, Tehran, Iran*

[3]*Department of Occupational Health and Safety Engineering, Tehran Medical Sciences Branch, Islamic Azad University, Tehran, Iran*

Received 2024-12-07; Revised 2025-06-28; Accepted 2025-07-14

This paper is available on-line at *http://ijoh.tums.ac.ir*

ABSTRACT

Background: Research on Indoor Air Quality (IAQ) in residential settings is limited, despite its importance for occupant health—especially during pandemics like COVID-19. Computational Fluid Dynamics (CFD) is a valuable tool for assessing IAQ parameters. This study aims to apply CFD to simulate air movement and velocity patterns in a living room to identify strategies for reducing coronavirus exposure.

Methods: A 3D model of a living room was created using GAMBIT software. Airflow simulations were performed using ANSYS FLUENT. The CFD model was validated by comparing computed air velocities with experimental measurements. Twelve scenarios were simulated, considering four different air supply locations and three Air Changes per Hour (ACH) rates (3, 6, and 8).

Results: The validation showed a maximum error of 14% and a root mean square error of 0.1 for air velocity, confirming the model's accuracy. Analytical calculations for a 10 µm particle showed a terminal settling velocity of 0.302×10^{-2} m/s and stopping distances of 0.0089 m and 0.011 m for breathing and talking, respectively. The highest mean air velocity (0.31 m/s at 1.1 m height) was achieved in Scenario 4 with an ACH of 8.

Conclusion: The location of the air supply and the ventilation rate significantly impact airflow patterns and can reduce exposure to airborne pathogens. Using mechanical ventilation and avoiding family gatherings are crucial for exposure control. The findings suggest that strategic ventilation design is essential for creating healthier indoor environments during a pandemic.

KEYWORDS: *CFD simulation, Air velocity, Airflow pattern, Living room, Coronavirus*

Corresponding author: *Majid Bayatian*

E-mail: *majid_bayatian@yahoo.com*

INTRODUCTION

Indoor Air Quality (IAQ) is a critical factor for human health, particularly in residential environments where people spend a significant portion of their time. The COVID-19 pandemic highlighted the risks associated with indoor spaces, as respiratory diseases can spread through bioaerosols generated by human activities such as breathing and talking. These airborne particles can carry viruses, and their transmission is strongly influenced by indoor air movement and ventilation [1-4].

Ventilation is a primary engineering control for mitigating airborne transmission indoors. Key factors include the ventilation rate, typically measured in Air Changes per Hour (ACH), and the airflow pattern within a room. Higher ACH values can reduce the concentration of airborne contaminants, thereby lowering the risk of infection. For living rooms, an ACH of 3–8 is often recommended. However, simply increasing the ventilation rate is not always sufficient; the pattern of air distribution—affected by the location of air supplies and exhausts, furniture, and heat sources—is equally important [5-7].

While the importance of ventilation is known, there is a knowledge gap in understanding detailed airflow dynamics in complex residential settings. Traditional measurement methods can be costly and provide limited data. Computational Fluid Dynamics (CFD) offers a powerful and cost-effective alternative for studying IAQ. CFD solves fundamental equations of fluid flow to predict airflow patterns, velocity fields, and other parameters in detail. It allows for the systematic evaluation of different ventilation strategies without physical modifications. Previous studies have used CFD to assess ventilation in hospitals and other public spaces, but fewer have focused on typical residential living rooms [8-11].

This study addresses this gap by using a validated CFD model to simulate airflow in a furnished living room occupied by several people. The objective is to investigate how different air supply locations and ACH rates influence air velocity and distribution patterns, particularly during autumn and winter, when natural ventilation is often minimal. The goal is to identify effective ventilation strategies to reduce the potential for coronavirus exposure in a home environment.

Materials and Methods

Case study

The case study was carried out in a living room with dimensions of 7 m × 5 m × 2.5 m in the x, y, and z directions, respectively, and included 8 occupants. To simulate and analyze the effect of air velocity and air supply location on the airflow pattern, 3D simulations were applied. In this living room, air is continuously supplied from the bottom of the entrance door, and two radiators serve as heat sources for the room (Fig. 1).

Geometry generation

GAMBIT software was used for geometry building and meshing (Fig. 1). Due to the complex geometry of the

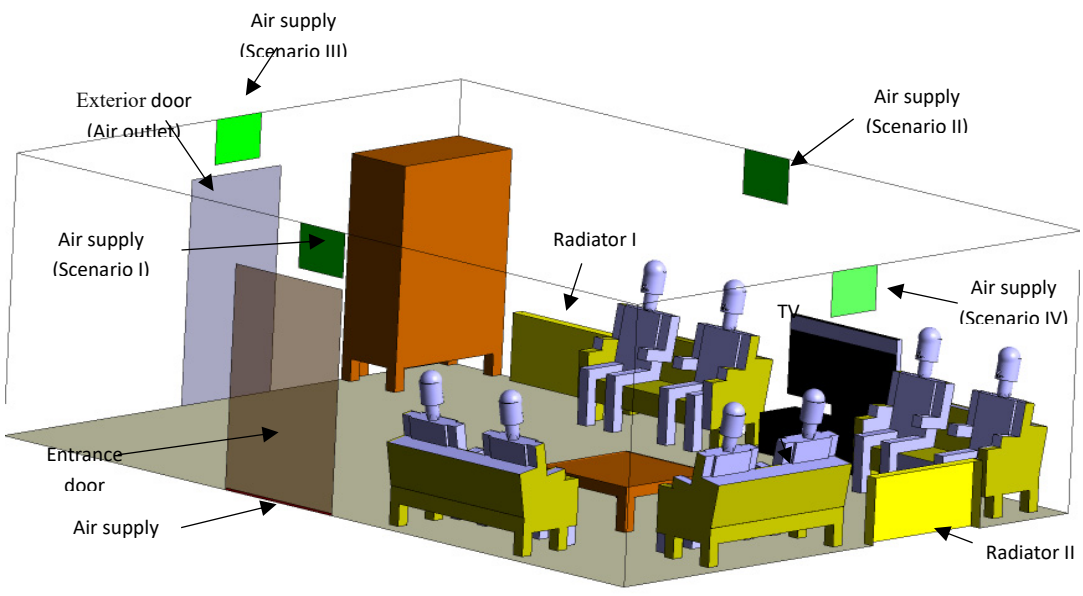

Figure 1. Geometry of computational domain

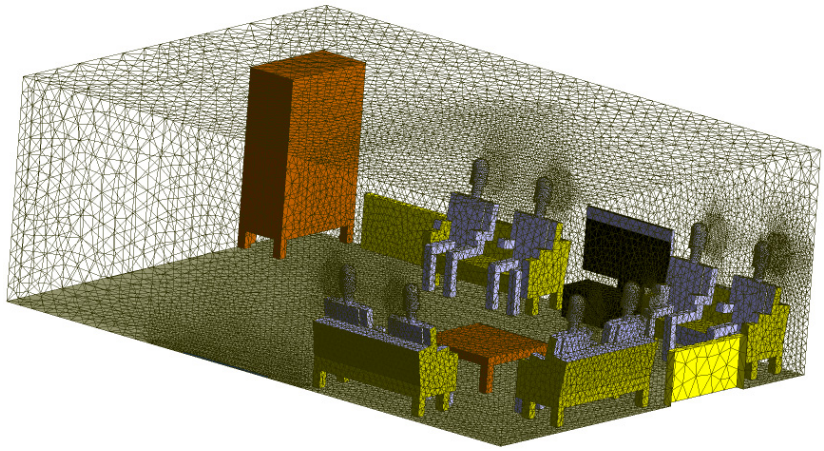

Figure 2. Isometric view of the surface mesh of the flow domain

Table 1. Mesh characteristics of five cases in mesh independency study

cases	Mesh No.	Node No.	Min. grid spacing (m)	Max. grid spacing (m)
A	515080	95981	0.030	0.50
B	890761	169540	0.025	0.40
C	1153472	210171	0.020	0.35
D	1416884	251307	0.020	0.33
E	1564255	278773	0.020	0.30

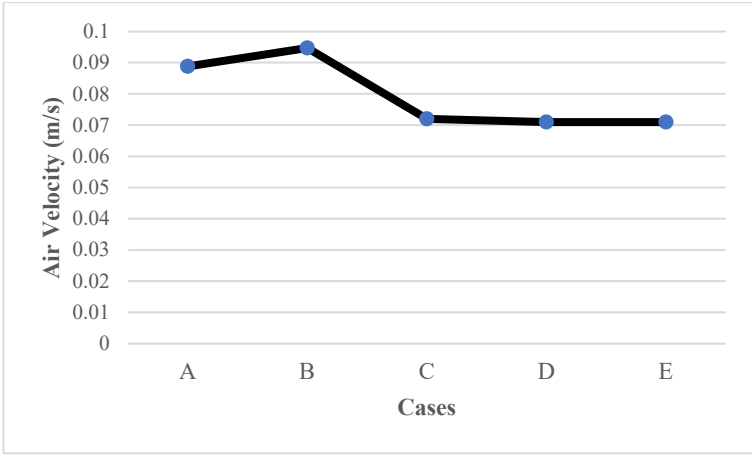

Figure 3. The effects of the cell number on the average air velocity

case study, the numerical domain was divided into 31 sub-region blocks, and a combination of unstructured and structured grid systems was applied. Mesh generation was performed using a T-grid algorithm with tet/hybrid elements (Fig. 2) in each block, and the meshes were adjusted at the boundaries of the blocks.

For the mesh independence study, five different mesh configurations, labeled A to E, with characteristics shown in Table 1, were tested. The mesh independence analysis ensured that the flow fields within the computational domain were not affected by mesh dimensions [12]. As shown in Figure 3, the final mesh consisted of 1,416,884 elementary cells. In this configuration, the cell spacing ranged from 0.02 m (near occupants and air supply) to 0.33 m (far from occupants and air supply).

Boundary conditions

Boundary conditions specify the properties of the surfaces within the computational domain and are

Table 2. Summary of boundary conditions

Boundary	Type	Notes
Air inlet	Inlet velocity	V=2.3m/s, Location: bottom of the entrance door
Air outlet	outflow	
Radiators	Wall	T= 345 K
Air inlet	Inlet velocity	V=2 m/s, Location: exhaled of occupants
Obstacles	Wall	No-slip conditions (include: furniture and TV)
Air inlet	Inlet velocity	Refer to the Scenario section
Occupants body	Wall	T= 308 K

required to fully define the airflow simulation. The operating pressure and density were set to 101,325 Pa and 1.19 kg/m³, respectively, and the thermal expansion coefficient was considered to be 0.003 K^{-1}. The inlet boundary condition was defined as a uniform velocity of 2.3 m/s, calculated based on experimental measurements. Table 2 presents the boundary conditions used in this study [13,14].

Governing equation

In the present study, the commercial package ANSYS FLUENT 16 was used to solve all governing equations, including conservation of mass (1), momentum (2), energy (4):

$$\nabla .V = 0 \quad (1)$$

$$\rho V.\nabla V = -\nabla P + \mu_{eff}\nabla^2 V + \rho g\beta\left(T - T_{ref}\right) \quad (2)$$

where P is pressure, ρ the air density, V the velocity, β the thermal expansion coefficient of air, μ_{eff} the effective dynamic viscosity, g the gravity acceleration, T_{ref} the temperature of a reference point, t the temperature. The turbulent influences are lumped into the effective viscosity as the sum of the turbulent viscosity μ_t and laminar viscosity μ_l :

$$\mu_{eff} = \mu_t + \mu_l \quad (3)$$

$$\rho C_p V.\nabla T = \lambda_{eff}\nabla^2 T \quad (4)$$

where C_p is the specific heat at constant pressure (J/kg °C) and λ_{eff} is the effective thermal conductivity (W/m °C) which can be expressed as:

$$\lambda_{eff} = \lambda_l + \lambda_t \quad (5)$$

where λ_l is the laminar thermal conductivity and λ_t is the turbulent thermal conductivity which depends on the local flow field.

Airflow pattern calculations use the Boussinesq approximation for thermal buoyancy. This approximation treats air density as constant in the momentum equations and accounts for the buoyancy effect on air movement through the difference between local air weight and the pressure gradient. Moreover, in this study, the standard *k–ε* turbulence model was used, with the governing equations for *k* (Equation 6) and *ε* (Equation 7) as follows:

$$\frac{\partial}{\partial x_i}\left(\rho u_i k\right) = \left(\mu + \frac{\mu_t}{\sigma_k}\right)\nabla^2 k + \mu_t S^2 - \rho\varepsilon \quad (6)$$

$$\frac{\partial}{\partial x_i}\left(\rho u_i \varepsilon\right) = \left(\mu + \frac{\mu_t}{\sigma_\varepsilon}\right)\nabla^2 \varepsilon + C_{\varepsilon 1}\frac{\varepsilon}{k}\mu_t S^2 - C_{\varepsilon 2}\rho\frac{S^2}{k} \quad (7)$$

$$\mu_t = \frac{\rho C_\mu k^2}{\varepsilon} \quad (8)$$

where coefficients $C_\mu, \sigma_k, \sigma_\varepsilon, C_{\varepsilon 1}$ *and* $C_{\varepsilon 2}$ are 0.09, 1.0, 1.3, 1.44 and 1.44, respectively, and $S = (S_{ij}S_{ji})^{0.5}$

Solver settings

In the present work, the continuity and the incompressible Navier-Stokes equations with gravitational force as well as the energy equation for the airflow pattern were numerically resolved. The flow was in a steady state without any reaction. The SIMPLEC algorithm was utilized for pressure-velocity coupling. Also, Persto, and QUIK schemes were used for the pressure terms, and the other variables, respectively.

CFD model validation

The CFD results need to be validated against relevant experiments [15]. Therefore, to validate the simulation, air velocity was measured within the computational domain. Measurements were carried out using two thermal anemometers (Kimo VT100 model). Finally, the CFD model results were compared with the

Table 3. Summary of parameters considered in simulations

Scenarios	ACH (h^{-1})	Inlet velocity (m/s)	Scenarios	ACH (h^{-1})	Inlet velocity (m/s)
I	3	0.37	III	3	0.37
	6	0.74		6	0.74
	8	0.975		8	0.975
II	3	0.37	IV	3	0.37
	6	0.74		6	0.74
	8	0.975		8	0.975

Table 4. Particle dynamics parameters for 10 diameter particle in breathing and talking

	V_i (m/s)	Re_p	C_D*	F_D (N)**	S (m)
Breathing	2	1.3	22.96	0.98×10^{-14}	0.0089
Talking	3.9	2.6	13.73	0.58×10^{-14}	0.011

*C_D is the Drag Coefficient (dependent on the Re_p), dimensional less
** F_D is Drag Force

measured air velocities using root mean square error and regression statistical tests [16].

Scenarios

The air change rate refers to the rate at which all the air inside a room is replaced by the ventilation system. It is calculated based on the airflow from each ventilation system inlet relative to the total volume of the room and is expressed in changes per hour.

$$ACH = \frac{Q}{V} \tag{9}$$

where Q is the inlet flow rate (m^3/h), and V the room volume (m^3). For the living room, ACH is 3-8 [17] [7]. This study considered the four air supply in the walls (Fig.1) for three different ACH levels (3, 6, and 8). Therefore, simulations were carried out for 12 cases (Tab 3). The air supply dimension was 0.4m×0.5m in the x,z and y,z axis, respectively. Therefore, air velocity in the inlet opening area were 0.37, 0.74 and 0.975 m/s for ACHs of 3, 6 and 8, respectively. Air exchange out the frequency in minutes (n_m) can be calculated as $n_m = \frac{60}{n}$, where n is ACH. Therefore, n_m was 20, 10 and 7.5 min for ACHs equal to 3, 6 and 8, respectively. Moreover, because airflow can result in thermal discomfort in the living room, the thermal environmental conditions for occupants were analyzed according to the graphical elevated air velocity method in ANSI/ASHRAE standard 55-2010 [18] via means of predicted mean vote (PMV) and predicted percentage of dissatisfied (PPD) [19].

Analytical Solution

Coronavirus is transmitted via infected microscopic airborne particles and contaminated aerosol droplets. Small particles and droplets of varying diameters are generated during talking and breathing, with a maximum particle size of 10 µm observed during talking [20]. The exhaled air velocity during breathing and talking is approximately 2 m/s and 3.9 m/s, respectively [21]. Accordingly, we calculated the particle Reynolds number (Equation 10), relaxation time (the time required for a particle to return to equilibrium after a disturbance; Equation 11), stopping distance (the maximum distance a particle with an initial velocity will travel in still air without external forces; Equation 12), and terminal settling velocity (the terminal free-fall velocity of the particle after release in still air; Equation 13) for particles with a 10 µm diameter under breathing and talking conditions:

$$Re_p = \frac{\rho V_r d_p}{\mu} \tag{10}$$

$$\tau = \frac{\rho_p d_p^2 C_c}{18\mu} \tag{11}$$

$$S = \frac{\rho_p d_p^2 C_c}{18\mu} V \tag{12}$$

$$V_{TS} = \frac{\rho_p d_p^2 g C_c}{18\mu} \tag{13}$$

where d_p is the particle (µm), V_r the relative velocity of the particle to the fluid, ρ_p the particle density (Kg/m^3), μ the viscosity (Pa. s), C_c the Cunningham correction factor, Re_p the particle Reynolds number, τ the relaxation time, S the stopping distance (m) and V_{TS} the terminal settling velocity of particles (m/s)[22].

RESULTS

This section presents the analytical calculations, the validation of the numerical model, and the simulation results for the 12 defined cases.

Analytical Solution for Particle Dynamics

Since particles with a diameter of 10 µm are predominantly produced during breathing and talking, key particle dynamic parameters were calculated analytically. The results are summarized in Table 4. The terminal settling velocity (VTS) for a 10 µm particle was calculated as 0.302×10^{-2} m/s, and the relaxation time (τ) was 0.0308×10^{-2} s. The stopping distance—defined as the maximum distance a particle travels in still air—was 0.0089 m for breathing and 0.011 m for talking.

Particle exhaust velocity $V(t)$ at any given time from the mouth depends on the initial velocity, relaxation time, terminal settling velocity, and particle exhaust time t. This velocity can be determined for breathing (Equation 14) and talking (Equation 15) as follows:

Breathing:

$$V(t)=0.302\times10-2+1.99\exp(0.0308\times10-2-t) \quad (14)$$

Talking:

$$V(t)=0.302\times10-2+3.89\exp(0.0308\times10-2-t) \quad (15)$$

Where t is time (s). By using these equations, particle exhaust velocity from the mouth can be calculated at any time. When t>>τ, V(t)=VTS. Theoretically, V(t) never reaches its terminal settling velocity, but in practice, V(t) reaches 63.2% of (VTS−Vi) when t=τ, and 99.3% of (VTS−Vi) when t=5τ.

CFD Model Validation

To validate the simulation results, air velocity was measured at several points within the living room at a height of 1.1 m (Fig. 4). The measured values were compared with those predicted by the CFD model at the same locations. The comparison between measured and simulated data is also illustrated in the Q–Q plot shown in Figure 5. The analysis yielded a maximum error of 14% and a root mean square error (RMSE) of 0.10. These results indicate that the model demonstrates good validity and can be reliably used to simulate the defined scenarios.

Simulation of Ventilation Scenarios

Simulations were performed for a baseline case (actual condition with minimal ventilation) and twelve scenarios with varying air supply locations and ACH rates. Under the actual condition (no mechanical ventilation), the mean air velocity at the 1.1 m inhalation height was very low—approximately 1.4×10^{-3} m/s. Figures 6 and 7 illustrate the mean air velocity at 1.1 m height for all scenarios. The results consistently show that as the ACH increases from 3 to 8, the mean air velocity in the room increases across all four scenarios. The highest mean air velocity, 0.31 m/s, was observed in Scenario IV with an ACH of 8.

Thermal comfort criteria, including Predicted Mean

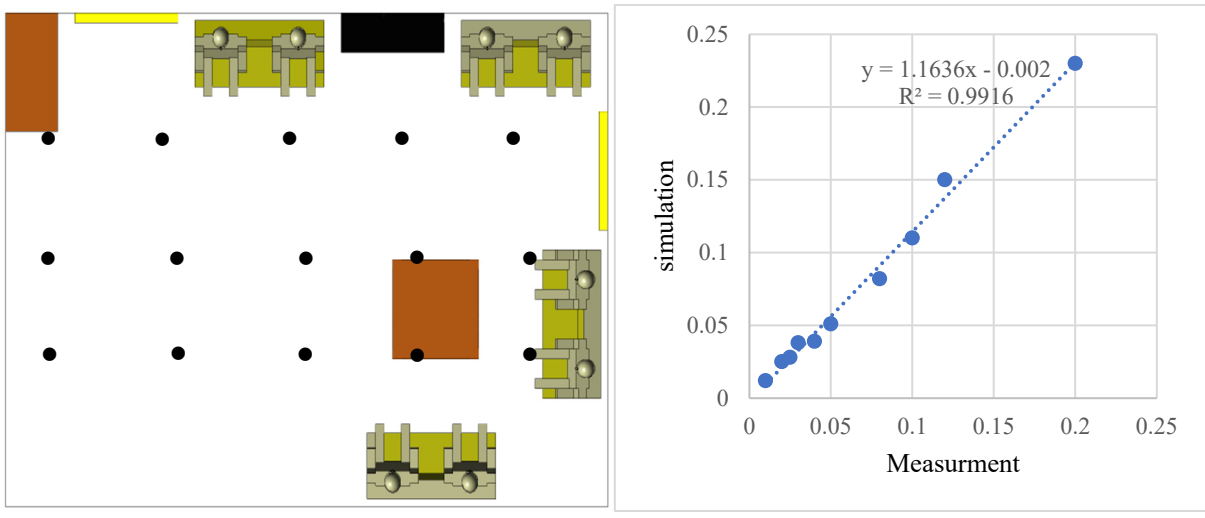

A **B**

Figure 4. Location of air velocity sampling points (•) (y=1.1m) **B:** Q-Q plot of air velocity (m/s)

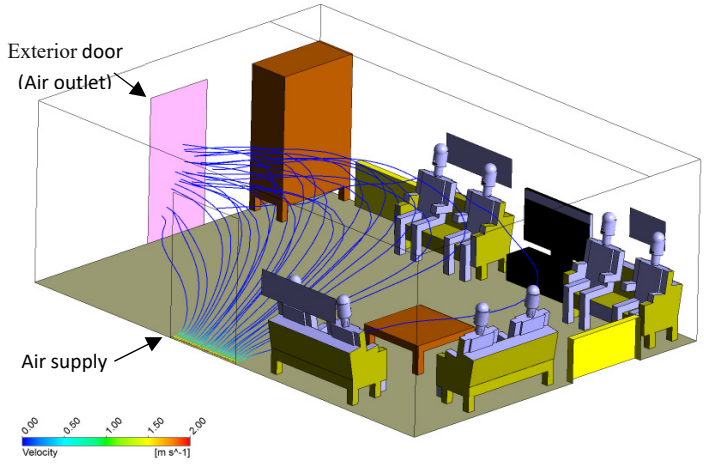

Figure 5. Airflow pattern and streamlines of air velocity in the actual condition

Table 5. Comparison of Measured and Simulated Air Velocity for Model Validation

Sampling Point	Measured Velocity (m/s)	Simulated Velocity (m/s)	Relative Error (%)
1	0.15	0.17	13.3
2	0.22	0.20	9.1
3	0.18	0.16	11.1
4	0.25	0.24	4.0
5	0.12	0.13	8.3
6	0.28	0.32	14.0

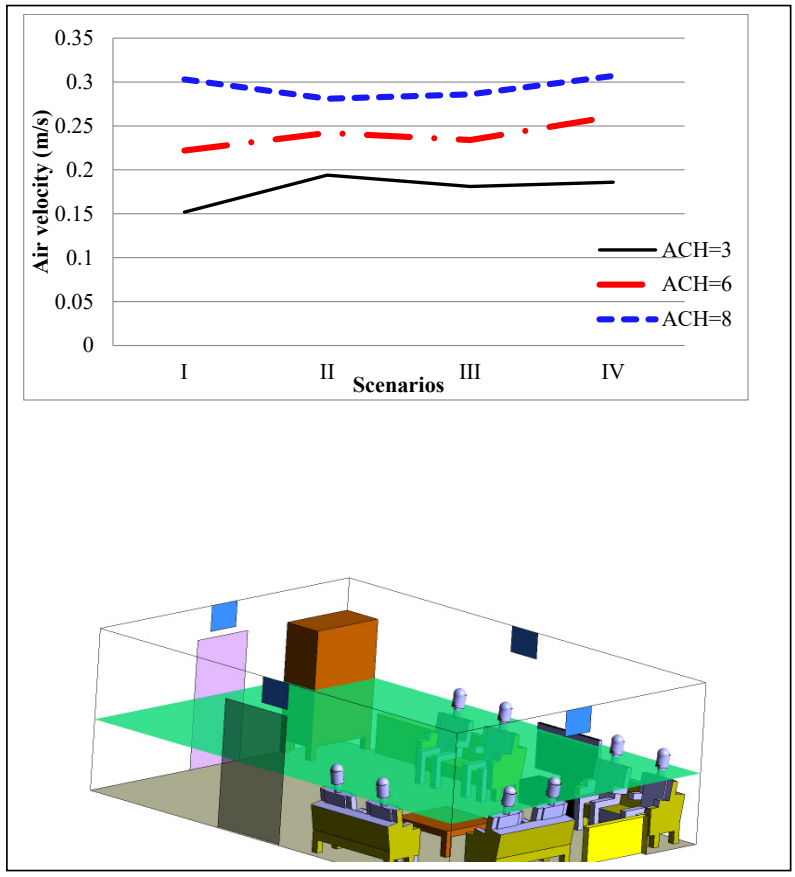

Figure 6. Mean air velocity in different air changes per hour at h=1.1 m at the Isosurface

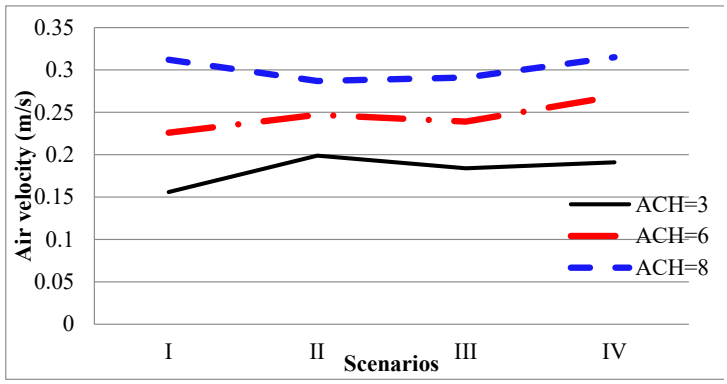

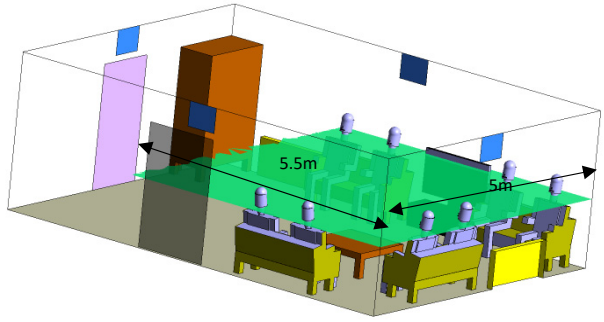

Figure 7. Mean air velocity in different air changes per hour at h=1.1 m at the plane

Table 6. Mean air velocity and thermal comfort criterias in all scenarios

Scenarios	ACH (h^{-1})	Comfort Zone	Mean Air Velocity (m/s)	PMV	PPD (%)	Scenarios	ACH (h^{-1})	Comfort Zone	Mean Air Velocity (m/s)	PMV	PPD (%)
I	3	SACZ*	0.154	0.4	8	III	3	SACZ	0.170	0.15	6
	6	LCNR**	0.236	0.31	7		6	LCNR	0.239	0.33	7
	8	LCNR	0.304	-0.14	5		8	LCNR	0.310	0.26	6
II	3	LCNR	0.199	0.18	6	IV	3	SACZ	0.176	0.41	9
	6	LCNR	0.262	0.27	7		6	LCNR	0.251	0.31	7
	8	LCNR	0.308	0.04	5		8	LCNR	0.311	0.1	5

* Still Air Comfort Zone
** Local Control Not Required

Vote (PMV) and Predicted Percentage of Dissatisfied (PPD), were also analyzed (Table 6). In all simulated scenarios, the conditions remained within the acceptable thermal comfort zone as defined by ASHRAE Standard 55 [19].

The trend of variation of air velocity in three ACH is almost the same in all scenarios; thus, the maximum air velocity is at the height of 1.2 m (Fig. 8). In ACH=8, the mean air velocity is higher and can have a sufficient effect on the spread of particles and microorganisms. However, in ACH=3, this effect is very low and can increase the mean age of the air in the living room. This mean age of the air (20 min) can have a significant effect on the infection of occupants.

Figure 9 illustrates the airflow streamlines for the four scenarios at ACH=8. Scenarios II and IV show more intense air mixing throughout the living room compared to Scenarios I and III.

Figure 10 shows the velocity vectors of air exhaled by the occupants. The velocity of exhaled air (2–3.9 m/s) is significantly higher than the ambient room air

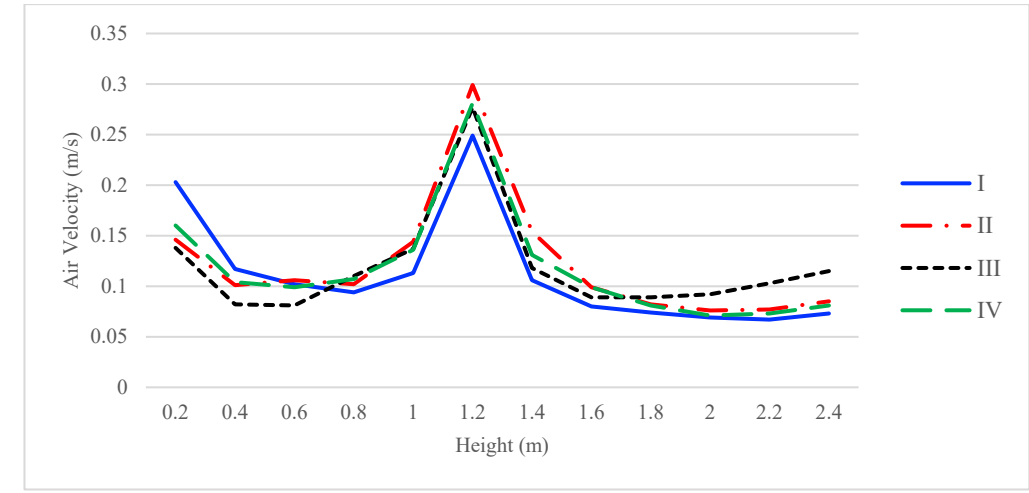

A

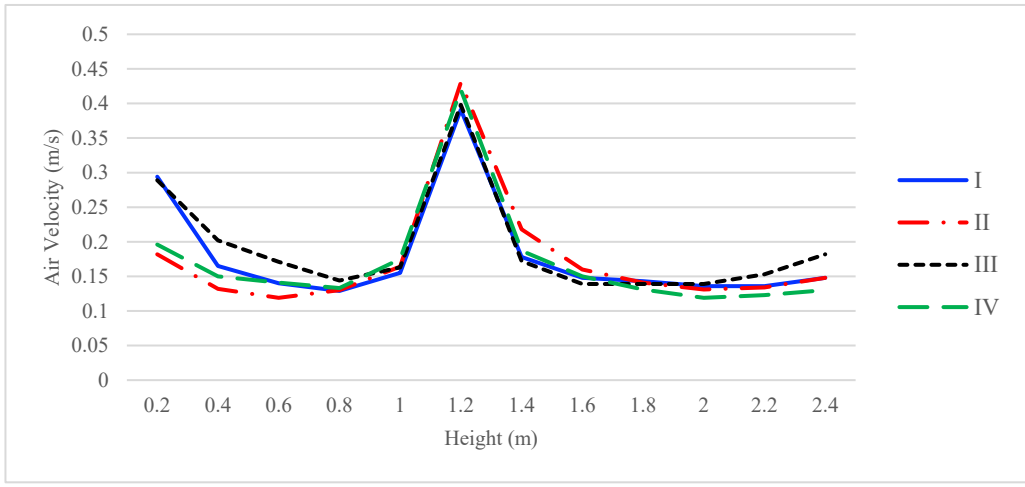

B

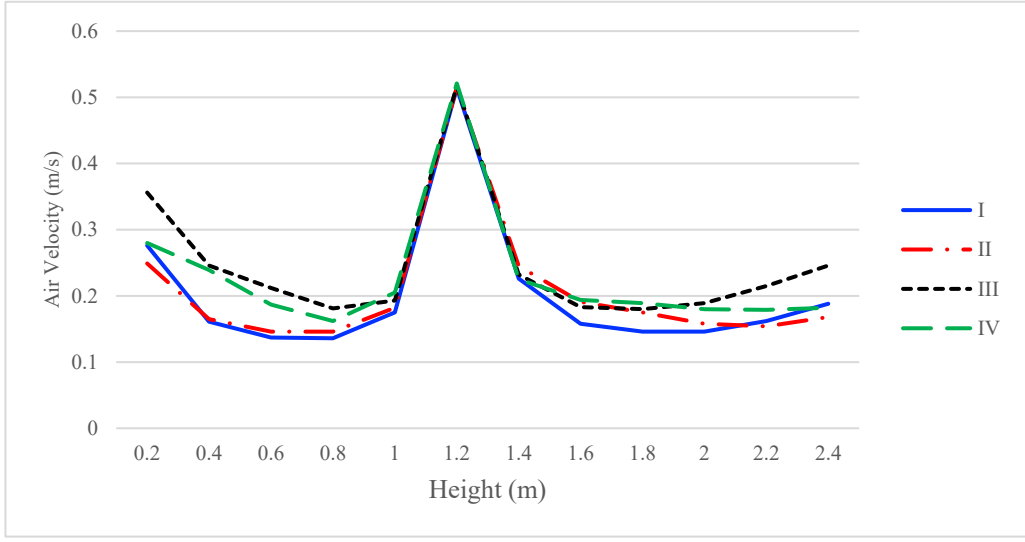

C

Figure 8. The variation of air velocity with height averaged on the isosurfaces, **A:** ACH=3, **B:** ACH=6, **C:** ACH=8)

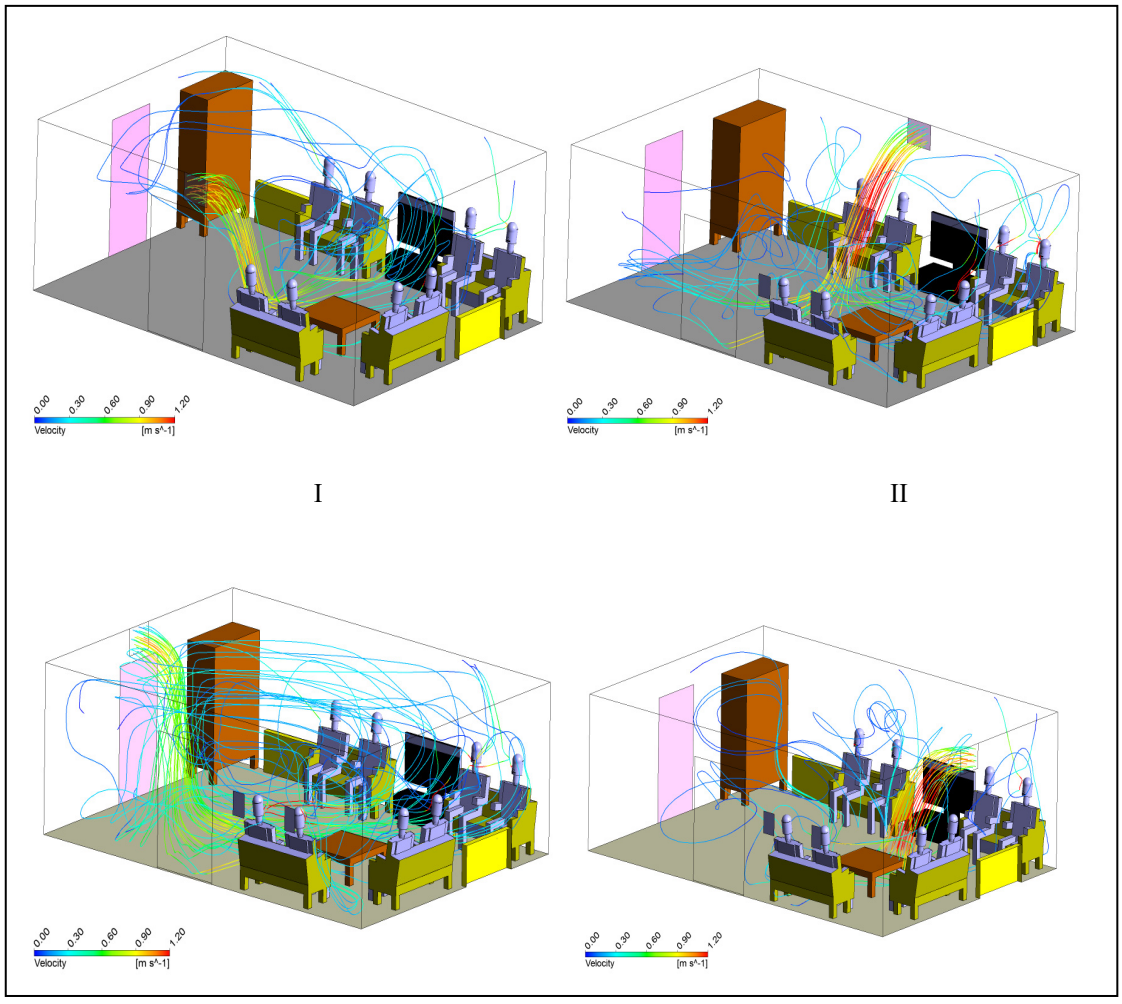

Figure 9. Airflow streamlines for 4 scenarios in ACH=8

velocity (approximately 0.3 m/s).

DISCUSSION

This study used a validated CFD model to assess how different ventilation strategies could reduce coronavirus exposure in a residential living room. The validation process confirmed the model's reliability, with a maximum error of 14% between simulated and measured data—acceptable for this type of analysis. The analytical results for particle dynamics provide important context. The calculated stopping distances of around 1 cm for 10 μm particles highlight that, without sufficient airflow, these particles can settle quickly near the source or remain suspended if they are smaller. This aligns with findings from other studies [23–25]. In the baseline case with no mechanical ventilation, the extremely low air velocity creates a stagnant environment where airborne particles can remain suspended for long periods, increasing the risk of inhalation and transmission among occupants.

The simulation results for the 12 scenarios demonstrate a clear relationship between ventilation and indoor air movement. Increasing the ACH from 3 to 8 consistently increased the mean air velocity in the breathing zone. Under conditions of low air velocity—such as at ACH = 3, where the mean age of air is 20 minutes—particles can remain suspended for longer periods, increasing the likelihood of inhalation by occupants. Conversely, increasing air velocity and turbulence, as seen at ACH = 8, enhances particle removal and reduces their concentration in the living room, resulting in a significant reduction in occupant exposure and, consequently, a lower risk of airborne transmission. This is consistent with evidence showing that poor ventilation contributes to virus spread [26–28].

The location of the air supply was also a critical factor. Scenario IV (with air supplied from the wall

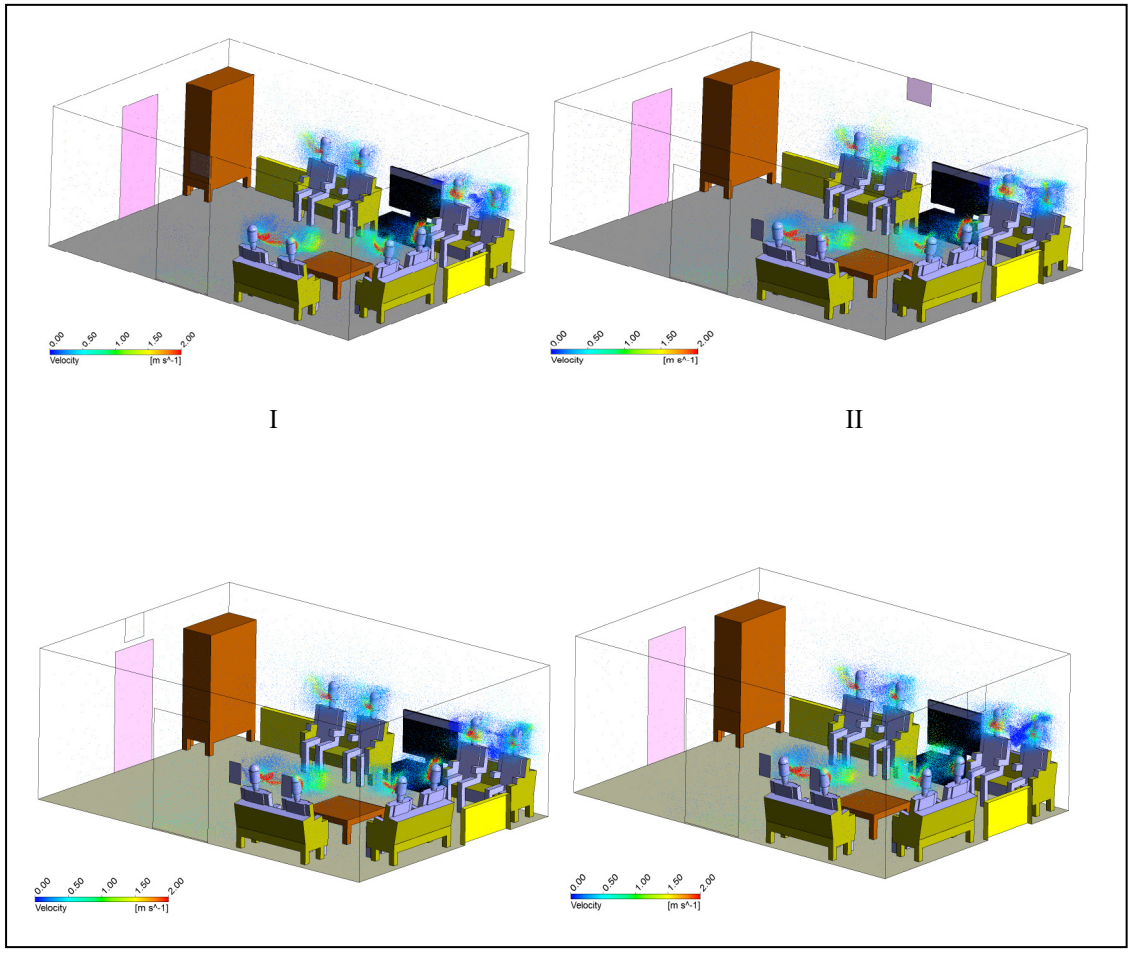

Figure 10. Vectors of air velocity in occupants exhale for 4 scenarios

behind the main sofa), combined with an ACH of 8, provided the highest mean air velocity and the most effective air mixing throughout the room. This intense mixing helps dilute and remove contaminated air from the occupants' breathing zones more effectively than other configurations. These findings support the recommendation that occupants should ideally be located near the fresh air supply to minimize inhalation of infectious aerosols [29].

While higher air velocity is beneficial for contaminant removal, it can potentially cause thermal discomfort. However, our analysis of PMV and PPD values showed that, even at the highest velocity (ACH = 8 in Scenario IV), the thermal environment remained within the comfort zone specified by ASHRAE standards. This indicates that effective contaminant control can be achieved without sacrificing occupant comfort [18, 19, 30].

The velocity of exhaled air from breathing or talking is much higher than the surrounding air velocity in the room. This creates a jet that can transport particles beyond the immediate vicinity of an infected person. Once the initial momentum of the jet dissipates, the fate of the particles is governed by the room's airflow pattern. Therefore, a well-designed ventilation system—such as that in Scenario IV—is crucial for capturing and removing these particles before they can spread throughout the space [21, 25].

Limitations and Future Studies

It is important to acknowledge the limitations of this study, which in turn provide directions for future research. This study inferred exposure risk from general airflow patterns rather than simulating individual particle trajectories. Future work could incorporate Lagrangian particle tracking models to more precisely predict the transport and deposition of aerosols of various sizes. Furthermore, the analysis focused on a single particle size (10 μm), whereas investigating a full spectrum of particle sizes could yield more comprehensive results. Another limitation was the assumption of static occupants and the exclusion of face mask usage. Future research, as also suggested in

the conclusion, could examine the impact of occupant movement and the use of different types of masks on contaminant dispersion patterns. Finally, the findings are specific to the geometry and layout studied; therefore, exploring different room sizes and furniture arrangements would help generalize the conclusions.

CONCLUSION

This study successfully used a validated CFD model to evaluate airflow patterns and their impact on reducing coronavirus exposure in a residential living room. The results demonstrate that both the ventilation rate (ACH) and the location of the air supply are critical factors in mitigating the risk of airborne transmission in indoor environments. The key findings indicate that poorly ventilated spaces pose a high risk for virus transmission. Increasing the air change rate to an ACH of 8 significantly improves air circulation. Furthermore, strategically placing the air supply to ensure effective mixing in occupied zones—as demonstrated in Scenario IV—is the most effective strategy for diluting and removing airborne contaminants. This can be achieved while maintaining thermal comfort for occupants. Based on these findings, it is strongly recommended that, during pandemics or outbreaks of respiratory diseases, family gatherings in enclosed spaces be avoided if possible. If gatherings do occur, implementing mechanical ventilation with an appropriate ACH and optimized airflow pattern is necessary to create a safer environment. These engineering controls should supplement other essential health protocols, such as social distancing and hygiene practices. Future research could explore the additional impact of wearing masks and varying occupant layouts.

ACKNOLWDEGMENT

The authors gratefully acknowledge the use of Gemini, a large language model developed by Google, for assistance with editing, grammar refinement, and improving the readability of the manuscript. The authors retain full responsibility for the final content and conclusions presented in this work.

FUNDING

This research did not receive any specific grant from funding agencies in the public, commercial, or not-for-profit sectors.

AVAILABILITY OF DATA AND MATERIALS

The raw data supporting the conclusions of this article will be made available by the corresponding author without restriction.

DECLARATION OF INTEREST

This manuscript was submitted as a pre-print in the link " https://assets.researchsquare.com/files/rs-316076/v1_covered.pdf?c=1631861661".

REFERENCES

1. Han L, Zhou W, Li W, Qian Y. Urbanization strategy and environmental changes: An insight with relationship between population change and fine particulate pollution. Sci Total Environ. 2018;642:789–799.
2. Luo N, Weng W, Xu X, Hong T, Fu M, Sun K. Assessment of occupant-behavior-based indoor air quality and its impacts on human exposure risk: A case study based on the wildfires in Northern California. Sci Total Environ. 2019;686:1251–1261.
3. Bhattacharyya S, Dey K, Paul AR, Biswas R. A novel CFD analysis to minimize the spread of COVID-19 virus in hospital isolation room. Chaos Solitons Fractals. 2020;139:110294.
4. Zhang D, Ortiz MA, Bluyssen PM. A review on indoor environmental quality in sports facilities: Indoor air quality and ventilation during a pandemic. Indoor Built Environ. 2022;doi:10.1177/1420326X221145862.
5. Sauermann. Air change rate: a vital measurement in the fight against COVID-19 [Internet]. 2020 [cited 2025 Oct 7]. Available from: https://sauermanngroup.com/en-INT/insights/air-change-rate-vital-measurement-fight-against-covid-19
6. Morawska L, Tang JW, Bahnfleth W, Bluyssen PM, Boerstra A, Buonanno G, et al. How can airborne transmission of COVID-19 indoors be minimised? Environ Int. 2020;142:105832.
7. Suwardi A, Ooi CC, Daniel D, Tan CKI, Li H, Liang OYZ, et al. The efficacy of plant-based ionizers in removing aerosol for COVID-19 mitigation. 2021.
8. Fareed Z, Iqbal N, Shahzad F, Shah SGM, Zulfiqar B, Shahzad K, et al. Co-variance nexus between COVID-19 mortality, humidity, and air quality index in Wuhan, China: New insights from partial and multiple wavelet coherence. Air Qual Atmos Health. 2020;13:673–682.
9. Ma N, Aviv D, Guo H, Braham WW. Measuring the right factors: A review of variables and models for thermal comfort and indoor air quality. Renew Sustain Energy Rev. 2021;135:110436.
10. Sosnowski M, Gnatowska R, Grabowska K, Krzywański J, Jamrozik A. Numerical analysis of flow in building arrangement: Computational domain discretization. Appl Sci. 2019;9(5):941.
11. Luo M, Guo J, Feng X, Chen W. Studying occupant's heat exposure and thermal comfort in the kitchen through full-scale experiments and CFD simulations. Indoor Built Environ. 2022;doi:10.1177/1420326X221147161.
12. Wen H, Malki-Epshtein L. A parametric study of the effect of roof height and morphology on air pollution dispersion in street canyons. J Wind Eng Ind Aerodyn. 2018;175:328–341.
13. Bayatian M, Azari MR, Ashrafi K, Jafari MJ, Mehrabi Y. CFD simulation for dispersion of benzene at a petroleum refinery in diverse atmospheric conditions. Environ Sci Pollut Res Int. 2021;doi:10.1007/s11356-021-13938-9.
14. Aziz MA, Gad IA, El Shahat F, Mohammed RH. Exper-

imental and numerical study of influence of air ceiling diffusers on room air flow characteristics. Energy Build. 2012;55:738–746.
15. Middha P. Development, use, and validation of the CFD tool FLACS for hydrogen safety studies. 2010.
16. Ni M, Wang H, Liu X, Liao Y, Fu L, Wu Q, et al. Design of variable spray system for plant protection UAV based on CFD simulation and regression analysis. Sensors (Basel). 2021;21(2):638.
17. Sauermann G. Air change rate: a vital measurement in the fight against COVID-19. 2020.
18. ASHRAE. Standard 55-2010: Thermal environmental conditions for human occupancy. Atlanta: American Society of Heating, Refrigerating and Air-Conditioning Engineers; 2010.
19. ASHRAE. Standard 55–2020: Thermal environmental conditions for human occupancy. Atlanta: American Society of Heating, Refrigerating and Air-Conditioning Engineers; 2020.
20. ISHRAE. COVID-19 guidance document for air conditioning and ventilation. 2020.
21. Xu C, Nielsen PV, Liu L, Jensen RL, Gong G. Human exhalation characterization with the aid of schlieren imaging technique. Build Environ. 2017;112:190–199.
22. Zhang Y. Indoor air quality engineering. Boca Raton: CRC Press; 2004.
23. Rohit A, Rajasekaran S, Karunasagar I, Karunasagar I. Fate of respiratory droplets in tropical vs temperate environments and implications for SARS-CoV-2 transmission. Med Hypotheses. 2020;144:109958.
24. Singh N, Kaur M. On the airborne aspect of COVID-19 coronavirus. arXiv Prepr arXiv:2004.10082. 2020.
25. Wei J, Li Y. Enhanced spread of expiratory droplets by turbulence in a cough jet. Build Environ. 2015;93:86–96.
26. Bhagat RK, Wykes MD, Dalziel SB, Linden P. Effects of ventilation on the indoor spread of COVID-19. J Fluid Mech. 2020;903.
27. Contini D, Costabile F. Does air pollution influence COVID-19 outbreaks? Multidiscip Digit Publ Inst. 2020.
28. Klompas M, Baker MA, Rhee C. Airborne transmission of SARS-CoV-2: theoretical considerations and available evidence. JAMA. 2020.
29. Guo M, Xu P, Xiao T, He R, Dai M, Zhang Y. Review and comparison of HVAC operation guidelines in different countries during the COVID-19 pandemic. Build Environ. 2020;doi:10.1016/j.buildenv.2020.107368.
30. Gupta D, Khare VR. Natural ventilation design: Predicted and measured performance of a hostel building in composite climate of India. Energy Built Environ. 2021;2(1):82–93.